

### Mechanism of Insertion of Isocyanides Across the Pd–C Bond in the Pyridyl Complex [PdCl{C<sub>5</sub>H<sub>3</sub>N-(6-Cl)-C<sup>2</sup>} (Diphos)] (Diphos = 1,2-Bis(diphenylphosphino)ethane)

A. CAMPAGNARO, A. MANTOVANI

Istituto di Chimica Industriale, Via Marzolo 9, 35100 Padua, Italy

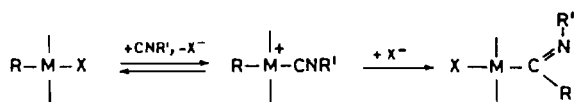
and P. UGUAGLIATI

Centro di Chimica e Tecnologia Composti Metallorganici C.N.R. c/o Istituto di Chimica Industriale, 35100 Padua, Italy

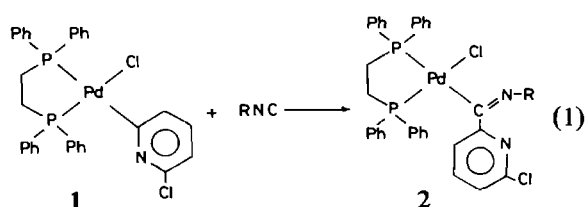
Received December 5, 1984

The insertion of isocyanides across M–C  $\sigma$ -bonds in alkyl and aryl platinum(II) and palladium(II) complexes has recently attracted much attention [1]. Such reaction has a bearing on the more general insertion processes of small molecules into transition metal–carbon  $\sigma$ -bonds, which are thought to be important intermediate steps in catalytic reactions. The use of isocyanides RNC, isoelectronic with carbon monoxide, allows a study of electronic and steric effects affecting the insertion, through a proper choice of the alkyl or aryl group R. In some systems double insertion of isocyanides may take place via insertion of one further isocyanide molecule across the metal–carbon bond of the iminoacyl complex resulting from the primary insertion process [2].

Very few mechanistic studies have been reported so far for this type of reaction [3, 5]. In general, prior coordination of the isocyanide to the metal upon displacement of halide ion is assumed, followed by insertion of the coordinated isocyanide across the M–C bond, possibly through migration of the alkyl or aryl group:



We have carried out a kinetic investigation of the insertion of RNC (R = C<sub>6</sub>H<sub>11</sub>, Bu<sup>t</sup>) into the Pd–C  $\sigma$ -bond of the pyridyl complex **1** [7] in dichloromethane (DCM) or 1,2-dichloroethane (DCE) at various



temperatures. The pyridyl substrate **1** proved well-suited for mechanistic studies, since the presence of the chloride substituent in the pyridyl ring slows down the insertion step and makes the system amenable to kinetic investigations by stabilizing the Pd–pyridyl linkage. The results are described below.

### Results and Discussion

#### Halide Displacement Equilibria

When studying reaction **1** under kinetic conditions, *i.e.* with an excess of isocyanide over the substrate **1**, we observed an immediate conversion of the spectrum of **1** in the range 400–280 nm into the spectrum of a new intermediate species, which subsequently reacted very slowly to yield the final imino complex **2**. The spectral changes related to the preliminary fast step are shown in Fig. 1 for a range

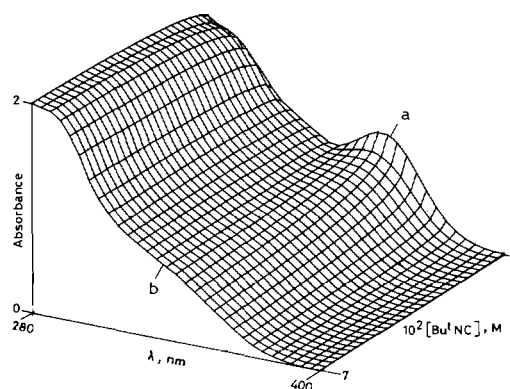
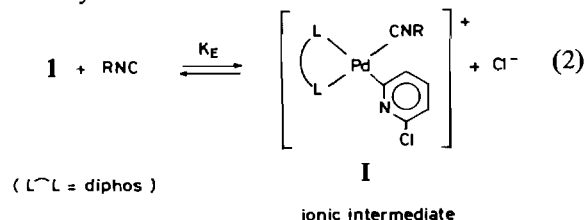


Fig. 1. 3-D representation of spectral changes corresponding to equilibrium (2) in DCM at 25 °C from non-linear regression of absorbance data according to model in eqns. (3)–(5). (a) Spectrum of **1**  $7.7 \times 10^{-5}$  M. (b) Spectrum of reaction mixture (mostly intermediate I) in the presence of Bu<sup>t</sup>NC  $7.0 \times 10^{-2}$  M.

of isocyanide concentrations. The initial molar conductance of a  $1 \times 10^{-4}$  M solution of **1** in DCE in the presence of Bu<sup>t</sup>NC  $1 \times 10^{-2}$  M at 40 °C was found to be  $77 \Omega^{-1} \text{cm}^2 \text{mol}^{-1}$  ( $\Lambda_{\text{M}} = 79 \Omega^{-1} \text{cm}^2 \text{mol}^{-1}$  for **1**) =  $7.8 \times 10^{-5}$  M and [Bu<sup>t</sup>NC] =  $7.5 \times 10^{-2}$  M in dichloromethane at 40 °C). This indicates that the halide replacement equilibrium takes place initially:



Abstract factor analysis [8] of the spectral changes of Fig. 1 confirms the presence of only two species absorbing in the wavelength range of study, viz., the substrate **1** and the ionic intermediate **I** ( $\text{Bu}^t\text{NC}$  does not absorb in such range). Spectral changes in Fig. 1 were analyzed quantitatively in order to determine the equilibrium constant  $K_E$  in reaction 2, in the following way: let  $M = \mathbf{1}$ ,  $L = \text{Bu}^t\text{NC}$ ,  $ML = \mathbf{I}$ . Then:

$$K_E = \frac{[\text{ML}][\text{Cl}^-]}{[\text{M}][\text{L}]} \quad (3)$$

$$[\text{M}] + [\text{ML}] = a$$

$$[\text{L}] + [\text{ML}] = b$$

$$[\text{ML}] = [\text{Cl}^-]$$

$$[\text{ML}] = \frac{(1/2) \{ (a+b) - [(a+b)^2 - 4ab(1+1/K_E)]^{1/2} \}}{(1-1/K_E)} \quad (4)$$

$$A_\lambda = \epsilon_\lambda^{\text{ML}}[\text{ML}] + \epsilon_\lambda^{\text{M}}[\text{M}] \quad (5)$$

were  $a$  and  $b$  are the total analytical concentrations of  $M$  and  $L$ , respectively,  $A_\lambda$  is the zero-time absorbance at wavelength  $\lambda$ ,  $\epsilon_\lambda$  is the molar extinction coefficient at  $\lambda$  (optical path length = 1 cm). The function minimized was:

$$\phi = \phi(\epsilon_i, K_E) = \sum (A_{\text{obs}} - A_{\text{calc}})^2$$

with  $\epsilon_\lambda^{\text{ML}}$  and  $K_E$  being the refined parameters. The values of  $\epsilon_\lambda^{\text{M}}$  were previously determined from solutions of pure  $M$ . No weighting scheme was applied. The minimization was carried out by an optimized version of Marquardt's [9] algorithm implemented on a Tektronix 4052 (64K) Graphic System [10]. Good starting guesses for the parameter vector were obtained by a preliminary Nelder-Mead Simplex search [11].

At convergence the parameter correlation matrix indicated that  $\epsilon_\lambda^{\text{ML}}$  and  $K_E$  are correlated, which resulted in the latter changing slightly with the wavelength. Therefore the non-linear fit was carried out for a series of wavelengths and the  $K_E$  values from individual fits were used to compute a weighted average value. It can be shown that this simplified procedure leads substantially to the same results as the more involved minimization of a multiresponse objective function [12]. Uncertainties quoted for  $K_E$  are averaged standard errors of the estimate. An example of the dependence of  $A_{340}$  on isocyanide concentration for the system  $\mathbf{1}/\text{Bu}^t\text{NC}$  in DCM at 30 °C is shown in Fig. 2, where the full line is the best fitting absorbance function (eqn. 5) computed with the optimized  $\epsilon_{340}^{\text{ML}}$  and  $K_E$  values from non-linear regression.

Table I lists the  $K_E$  values for the system of eqn. 2 in DCM and DCE ( $R = \text{Bu}^t\text{NC}$ ,  $\text{C}_6\text{H}_{11}$ ) at various temperatures, along with the thermodynamic parameters  $\Delta H^\circ$  and  $\Delta S^\circ$  derived from non-linear regression of  $K_E$  vs.  $T$  (weighting scheme  $w_1 = 1/\sigma_1^2$ ). The formula-

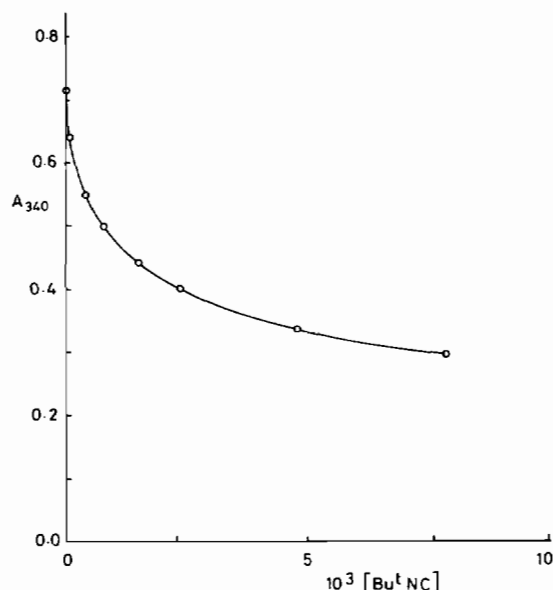


Fig. 2. Non-linear fit of absorbance at 340 nm vs.  $[\text{Bu}^t\text{NC}]$  for equilibrium (2) in DCM at 30 °C. Solid line is calculated from optimized parameters in model (3)–(5).

TABLE I. Equilibrium Constants and Thermodynamic Parameters for the Reaction 2:



Solvent	$T, ^\circ\text{C}$	$10^2 K_E$	Thermodynamic Parameters
DCM	15.0	$7.7 \pm 0.1$	$\Delta H_E^\circ = -13 \pm 2$ kcal/mol $\Delta S_E^\circ = -50 \pm 6$ e.u.
	20.0	$5.9 \pm 0.2$	
	25.0	$3.2 \pm 0.1$	
	30.0	$2.7 \pm 0.1$	
DCE	15.0	$10.8 \pm 0.2$	$\Delta H_E^\circ = -19 \pm 2$ kcal/mol $\Delta S_E^\circ = -72 \pm 6$ e.u.
	20.0	$4.5 \pm 0.1$	
	27.5	$2.4 \pm 0.1$	
	32.2	$1.5 \pm 0.1$	

tion of this model in which  $A = \exp(\Delta S^\circ/R - \Delta H^\circ/RT_0)$ ,  $B = +\Delta H^\circ/R$ ,  $K_E = A \exp(B/T^*)$ ,  $1/T^* = 1/T_0 - 1/T$ ,  $T_0 =$  average absolute temperature, has been shown to be particularly efficient in reducing the correlation between the parameters and improving their estimate [8a, 13].

The high correlation between the extinction coefficient of the intermediate and the equilibrium constant referred to above is a typically unavoidable feature of equilibrium studies based on spectrophotometric data measurements [14], which originates from the very nature of the mathematical model underlying the data reduction process. A large correlation coefficient will lead to large uncertainties in the parameters although the fit of observed to calculated data is satisfactory. Correlation coefficients are unfortunately independent of the accuracy of the

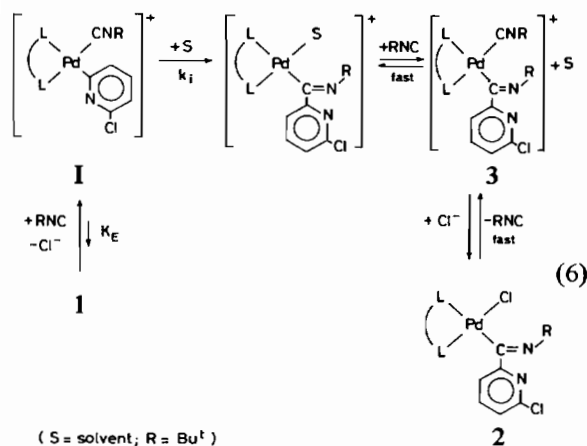
measured data and of the number of wavelengths at which measurements are made, and no prospects for reducing them exist other than widening the range of concentrations of ligand (L) being explored.

Attempts to evaluate the equilibrium constant  $K_E$  from conductivity data based on eqns. 3–4 gave a satisfactory non-linear fitting. However, the resulting  $K_E$  values were always of the same order of magnitude, but different from, those determined spectrophotometrically. This is likely to be due to the failure of the first-approximation model employed to account for probable ion-pairing and/or ionic strength effects. As can be seen from Table I, reversible formation of the ionic pyridyl–isocyanide intermediate **I** is an exothermic process characterized by an extremely negative standard entropy, in agreement with the generation of ionic species in solvents with appreciable dielectric constant.

The occurrence of ionic intermediates resulting from halide displacement by isocyanides was established in the course of insertion of isocyanides into the Pt–C bond of organoplatinum complexes of type *trans*-[PtX(R)(PR<sub>3</sub>)<sub>2</sub>] (X = halide; R = Me, Ph) [3]. No direct evidence has been presented so far for a similar step in the insertion in organopalladium substrates. It appears that the ease of halide replacement is related to the high *trans*-influence of ligands *trans* to the halide (*i.e.*, alkyl, aryl groups or tertiary phosphines, as in our substrate **1**), and to the good coordinating ability of the isocyanide.

### Insertion Kinetics

DMC or DCE solutions of the substrate **1** in the presence of excess Bu<sup>t</sup>NC undergo very slow insertion of the isocyanide across the Pd–pyridyl  $\sigma$  bond to give the iminoacyl derivative, which is in turn in fast equilibrium with a final chloride displacement product **3**:



Concentration conditions ( $[1]_0 = 7 \times 10^{-5}$  M;  $[\text{RNC}]$  in the range  $(1\text{--}15) \times 10^{-2}$  M; no Cl<sup>-</sup> added) are such as to ensure quantitative conversion of the

substrate **1** to the intermediate **I** upon mixing of the reactants and throughout the insertion process, as can be easily verified from eqns. 3–5. Spectral changes with time in the range 400–280 nm corresponding to the insertion stage in eqns. 6 for R = Bu<sup>t</sup>NC in DCE at 45 °C are shown in Fig. 3. The disappearance of intermediate **I** is a first order process, obeying rate law 7:

$$-\frac{d[\text{I}]}{dt} = k_i[\text{I}] \quad (7)$$

throughout the range of RNC concentrations studied.

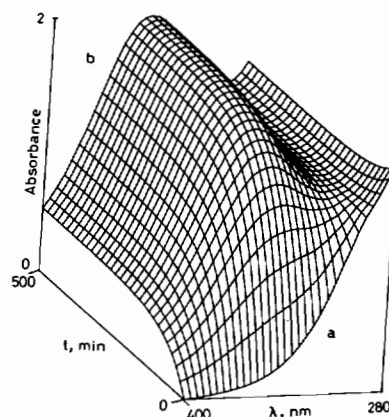


Fig. 3. 3-D representation of spectral changes for the insertion reaction (6) in DCE at 45 °C showing the dependence of absorbance with time from single exponential non-linear regression of  $A_t$  vs.  $t$  data. (a) Spectrum of starting solution containing the intermediate **I** (from  $1.7 \times 10^{-5}$  M and Bu<sup>t</sup>NC  $1.0 \times 10^{-1}$  M). (b) Spectrum of reaction mixture after *ca.* 7 half-lives.

No dependence of the constant on either excess isocyanide or added chloride ion (as AsPh<sub>4</sub>Cl) was detected.

The values of rate constants  $k_i$  were obtained by non-linear regression of absorbance vs. time data\*, according to the integrated form of eqn. 7,  $A_t = A_\infty + (A_0 - A_\infty)\exp(k_i \cdot t)$  ( $A_\infty$  = absorbance of the reaction mixture at the time of mixing;  $A_t$  = absorbance at the time  $t$ ). These values, which are averaged over several kinetic runs at different RNC concentrations, are listed in Table II which also contains the activation parameters from non-linear regression of  $k_i/T$  vs.  $1/T^{**}$  data according to the Eyring formalism in re-parametrized form [13] (Fig. 4).

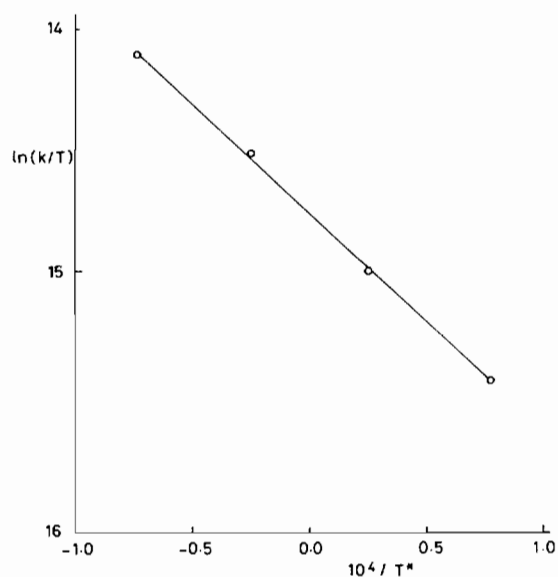
In the presence of excess isocyanide the spectrum of the reaction mixture after completion of the

\*All graphical and statistical analyses of equilibrium and kinetic data were carried out with a Tektronix 4052 (64 K RAM) Graphic System equipped with a 4907 File Manager Floppy Disk triple unit (1.8 MB) and a 4262 Digital Plotter, with locally-prepared chemometrics programs.

\*\*See footnote on p. L18.

TABLE II. Rate Constants and Activation Parameters for the Insertion of Bu<sup>t</sup>NC in 1 (eqn. 6).

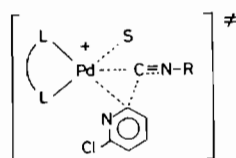
Solvent	T, °C	10 <sup>5</sup> k <sub>1</sub> , s <sup>-1</sup>
DCM	14.8	0.60 ± 0.02
	20.0	1.12 ± 0.01
	25.0	1.47 ± 0.03
	30.0	2.50 ± 0.01
		ΔH <sup>‡</sup> = 15 ± 2 kcal/mol
		ΔS <sup>‡</sup> = -30 ± 5 e.u.
DCE	35.0	6.30 ± 0.01
	40.0	10.00 ± 0.02
	45.0	16.20 ± 0.01
	50.0	24.20 ± 0.02
		ΔH <sup>‡</sup> = 17 ± 1 kcal/mol
		ΔS <sup>‡</sup> = -22 ± 2 e.u.

Fig. 4. Eyring plot for insertion of Bu<sup>t</sup>NC in DCE; 1/T\* = 1/T - 1/T<sub>0</sub> (T<sub>0</sub> = 315.66 K). Solid line is calculated from optimized activation parameters of linearized model in (k/T) = A + B/T\* [13].

reaction (7–8 half-lives) was superimposable with the spectrum of an independently prepared sample\* of the insertion product 2 in the presence of isocyanide under comparable concentration conditions.

\*cis-[PdClC(=NBU<sup>t</sup>){C<sub>5</sub>H<sub>3</sub>N(6-Cl)-C<sup>2</sup>}(diphos)] (2): from an equimolar mixture of 1 and Bu<sup>t</sup>NC in DCE under nitrogen at 40 °C for 2 d (cf. ref. 6). <sup>31</sup>P-<sup>1</sup>H NMR (CD<sub>2</sub>Cl<sub>2</sub>, δ/ppm downfield from 85% H<sub>3</sub>PO<sub>4</sub>): 48.3D, 26.9D; J<sub>P-P</sub> = 45 Hz. <sup>1</sup>H NMR (CD<sub>2</sub>Cl<sub>2</sub>, δ/ppm downfield from TMS): 1.21 S (CMe<sub>3</sub>). IR (Nujol): ν<sub>C=N(imino)</sub> 1620 cm<sup>-1</sup>; ν<sub>Pd-Cl</sub> 280 cm<sup>-1</sup>.

As can be seen, the intramolecular insertion step is accompanied by a fairly high activation enthalpy and a highly negative activation entropy, which reflect respectively the solvent assisted nature of the process and the decrease of freedom in the strongly oriented transition state involving migration of the pyridyl group onto the coordinated isocyanide moiety:



The insertion of isocyanides across the Pd–Me bond in *trans*-[PdMe(CNBU<sup>t</sup>)<sub>2</sub>I] in chlorobenzene or toluene was also found to be first-order in substrate concentration and to be independent of the nature of added nucleophile L (L = CNBU<sup>t</sup>, PPh<sub>3</sub>, P(OPh)<sub>3</sub>) [5], consistent with an unassisted intramolecular migration of the methyl group onto the isocyanide.

In a general way, the ease of insertion of isocyanides across metal–alkyl bonds increases with increasing electrophilic ability of the isocyanide and increasing nucleophilic character of the alkyl group, with the steric requirements around the reacting centers playing an adverse role [1]. Indeed, the presence of the very poorly nucleophilic Cl-substituted pyridyl group in substrate 1 and of the sterically demanding and poorly electrophilic Bu<sup>t</sup>NC in this study was instrumental in drastically reducing the rate of the insertion reaction step (eqn. 6). This made it possible to study quantitatively the establishment of fast pre-equilibria 2 prior to the onset of the subsequent insertion stage. Moreover, due to this low reactivity no evidence for multiple insertion of the excess isocyanide across the metal–C<sub>imino</sub> bond of 2, subsequent to the primary process, could be obtained under both preparative and kinetic conditions, at variance with what occurs with other systems [2, 4, 5].

The role of steric factors is borne out by the fact that the bulkier Bu<sup>t</sup>NC inserts somewhat slower than cyclohexylisocyanide (2.5 × 10<sup>-5</sup> s<sup>-1</sup> as compared to 3.0 × 10<sup>-5</sup> s<sup>-1</sup> at 30 °C in DCM).

Consistently, insertion of aliphatic and aromatic isocyanides on the palladium–thienyl bond in *trans*-[PdBr(thienyl)(PPh<sub>3</sub>)<sub>2</sub>] in DCE is comparatively much faster [15].

We are presently pursuing the kinetic study of this insertion reaction on the substrate *trans*-[PdCl{C<sub>5</sub>H<sub>3</sub>N(6-Cl)-C<sup>2</sup>}(PPh<sub>3</sub>)<sub>2</sub>]. Preliminary results indicate a higher insertion rate and the occurrence of phosphine–isocyanide ligand exchange processes.

## References

- 1 E. Singleton and H. E. Oosthuizen, *Adv. Organomet. Chem.*, **22**, 267 (1983).
- 2 Y. Yamamoto and H. Yamazaki, *Bull. Chem. Soc. Jpn.*, **44**, 1873 (1971).
- 3 P. M. Treichel, K. P. Wagner and R. W. Hess, *Inorg. Chem.*, **12**, 1471 (1973).
- 4 Y. Yamamoto and H. Yamazaki, *Inorg. Chem.*, **13**, 438 (1974).
- 5 S. Otsuka and K. Ataka, *J. Chem. Soc., Dalton Trans.*, 327 (1976).
- 6 A. Mantovani, *Monatsh. Chem.*, **114**, 1045 (1983).
- 7 A. Mantovani, *J. Organomet. Chem.*, **255**, 385 (1983).
- 8 a) L. Sandrini, A. Mantovani, B. Crociani and P. Uguagliati, *Inorg. Chim. Acta*, **51**, 71 (1981); b) P. Uguagliati, A. Benedetti, S. Enzo and L. Schiffini, *Comput. Chem.*, **7**, (1984) in press.
- 9 D. W. Marquardt, *J. Soc. Ind. Appl. Math.*, **2**, 431 (1963); T. Tabata and R. Ito, *Comput. J.*, **18**, 250 (1975).
- 10 'Tektronix PLOT 50 Statistics, Vol. IV' software package.
- 11 D. M. Olsson and L. S. Nelson, *Technometrics*, **17**, 45 (1975).
- 12 C. A. Brignoli and H. DeVoe, *J. Phys. Chem.*, **82**, 2570 (1978).
- 13 a) P. Uguagliati, R. Michelin, U. Belluco and R. Ros, *J. Organomet. Chem.*, **169**, 115 (1979) and refs. therein; b) R. R. Krug, W. G. Hunter and R. A. Grieger, *J. Phys. Chem.*, **80**, 2335 (1976).
- 14 P. J. Lingane and Z. Z. Hugus Jr, *Inorg. Chem.*, **9**, 757 (1970); T. O. Maier and R. S. Drago, *Inorg. Chem.*, **11**, 1861 (1972).
- 15 A. Mantovani, L. Calligaro and A. Pasquetto, *Inorg. Chim. Acta*, **76**, L145 (1983).